Printable 3D Carbon Nanofiber Networks with Embedded Metal Nanocatalysts

*Marcel Simsek,† Kilian Hoecherl,† Marc Schlosser,‡ Antje J. Baeumner† and Nongnoot Wongkaew†**

† Institute of Analytical Chemistry, Chemo- and Biosensors

University of Regensburg

Universitaetsstraße 31, 93053 Regensburg, Germany

‡ Institute of Inorganic Chemistry

University of Regensburg

Universitaetsstraße 31, 93053 Regensburg, Germany

KEYWORDS: carbon nanofibers; electrochemical sensors; electrospinning; laser-induced carbonization; nanocatalysts

ABSTRACT

Carbon nanofiber (CNF)-nanocatalyst hybrids hold great promise in fields such as energy storage, synthetic chemistry and sensors. Current strategies to generate such hybrids are laborious and utterly incompatible with miniaturization and large-scale production. Instead, this

work demonstrates that Ni-nanoparticles embedded in 3D CNFs of any shape and design can be easily prepared using electrospinning followed by laser carbonization under ambient conditions. Specifically, a solution of $Ni(acac)_2$/Polyimide is electrospun and subsequently a design is printed via CO_2 laser (Ni-LCNFs). This creates uniformly distributed small Ni nanoparticles (~ 8nm) very tightly adhered to the CNF network. Morphological and performance characteristics can be directly influenced by metal content and lasing power and hence adapted towards desired performance. Here, Ni-LCNFs are optimized for non-enzymatic electrochemical sensing of glucose with a great sensitivity of 2092 $\mu A\ mM^{-1}\ cm^{-2}$ and a detection limit down to 0.3 μM. Its selectivity for glucose versus interfering species (ascorbic and uric acid) is essentially governed by the Ni content. Most importantly, this strategy can be adapted to a whole range of metal precursors and hence provide opportunities for such 3D CNFs nanocatalyst hybrids in point-of-care applications where high performance but also sustainable and low-cost fabrication are of utmost importance.

INTRODUCTION

Carbon nanofiber (CNF)-metal nanocatalyst hybrids hold great promise in developing electrochemical devices applied to energy storage and conversion, e.g. batteries and supercapacitors, water splitting,[1] and sensors.[2] Utilizing CNFs as a support generally offers favorable features in promoting efficient electrocatalytic reactions.[3] In particular, three-dimensional (3D) architecture of CNF networks affords high surface area and porosity that significantly boost the internal mass transfer, thus facilitating efficient interactions between catalytic sites and electrolytes. Their good electrical conductivity, low material cost, chemical

inertness and high stability under harsh conditions are additional advantages that make CNFs widely used as a support of metal nanocatalyst.

In order to generate metal nanocatalyst-loaded CNFs various strategies have been proposed, e.g. electrodeposition,[4] chemical anchoring by functional groups,[5] chemical vapor deposition[6] or microwave-assisted synthesis.[7] Chemical or electrochemical reduction of metal precursors on CNFs are among the most popular methods. Even though great electrocatalytic performance of the resulting hybrids are achievable, those techniques are considerably tedious and have poor reproducibility, thus hampering their applicability in large-scale manufacturing. The oxidation of CNFs prior to metal reduction is often needed to ensure sufficient hydrophilicity for efficient anchoring catalyst particles.[3] Such treatment may, however, introduce an adverse effect in terms of electrical conductivity. Besides, the reduction of metal precursor onto porous CNFs may suffer from the poor adhesion strength owning to high roughness, and heterogeneity of oxygenate groups at CNF's edge sites. Thus, the reduced metal nanocatalyst obtained via these approaches may not be a suitable candidate for long-term uses or under mechanical forces such as stirred/flow conditions.

Electrospinning has currently gained tremendous attention in producing CNFs as it is highly compatible with industrial scale production and cost effective.[8] To produce CNFs, a solution of polymer precursor, e.g. polyacrylonitrile (PAN), is electrospun and subjected to a two-step heat treatment, i.e. stabilization and carbonization. The technique enables facile and efficient incorporation of metal precursor/s through just blending them with a solution of polymer precursor where the applied electric field could potentially promote uniform distribution of the metal precursors along the as-spun fibers. Upon two-step thermal treatment the formation of CNFs and metal nanoparticles can be readily obtained. As shown in several studies,[9–15] highly

uniform distribution and firmly embedment of metal nanocatalysts within CNFs can be realized via this strategy, which undoubtedly leads to remarkable electrocatalytic performance as well as great durability of the as-prepared hybrids that are successfully employed in various applications.

A growing demand of portable electrochemical devices in energy storages and conversions,[16,17] point-of-care diagnostics[18] and wearable sensors[19] has nowadays driven research efforts towards miniaturization and integration of functional nanomaterials. To meet this end, transfer-free, fully printed, customized electrode designs and roll-to-roll production feasibility are highly preferred. Metal nanocatalyst-loaded CNFs prepared via conventional heat treatment still cannot fulfil these preferences as they inevitably require laborious transfer and complicated integration approaches after their production.[10,14,15] Difficulty in maintaining 3D structures of the CNF networks remains an additional issue after device integration.

In contrast, laser-induced carbonization has become a promising technology to tackle those challenges. Various kinds and forms of substrate,[19] including electrospun nanofibers recently developed by our group,[20] have been laser-scribed into electrodes and investigated their performances both in energy-related fields and sensors. A study shown by Tour's group has revealed the possibility of CO_2 laser in converting polyimide (PI) film containing metal precursor into metal oxide nanocrystals embedded in graphene.[21] The hybrids exhibited excellent electrocatalytic activity and high cycling stability in converting O_2 to OH^-.

This work presents 3D CNF networks embedded with metal nanocatalysts realized by one-step laser carbonization of electrospun PI nanofibers containing metal precursor. Here, solvent soluble PI and a metal complex, $Ni(acac)_2$ as an example, were blended and electrospun on an indium tin oxide (ITO) coated plastic sheet. The as-spun nanofibers were subsequently

exposed to a CO_2 laser following the desired pattern of electrode design, termed as Ni-LCNFs. Ni content and lasing power were investigated to maximize degree of metal loading while maintaining electrospinnability as well as intact fibrous morphology. The strategy not only enabled remarkable adhesion stability between Ni nanocatalysts and LCNFs but also provided the Ni-LCNF electrodes with excellent electrocatalytic activity towards non-enzymatic glucose sensing with minimum interfering effect from uric acid (UA) and ascorbic acid (AA).

MATERIALS AND METHODS

Preparation of LCNF

Nanofiber mats were prepared by electrospinning of a solution containing 15 wt % Matrimid 5218 (Huntsman Advanced Materials BVBA, Belgium) and nickel(II) acetylacetonate (95 %, Sigma-Aldrich, Germany) or iron(III) acetylacetonate (≥99.9 % trace metals basis, Sigma-Aldrich, Germany) dissolved in N,N-dimethylacetamide (Merck, Germany). The metal salt percentages reported here are relative to the dry mass of the polymer. It is abbreviated $Ni(acac)_2$ or Ni (or Fe) in the other sections. Spinning solutions were ultrasonicated for 30 min and stirred at least overnight before spinning. The electrospinning was conducted for 15 min per fiber mat at a 10 μl min^{-1} flow rate with a 15 cm tip-to-collector distance. The applied voltage was adjusted in the range of 12-14 kV dependent on ambient temperature and humidity conditions. Indium tin oxide coated PET (ITO-PET, sheet resistivity 60 Ω/sq, 1 ft x 1 ft x 5 mil, Sigma Aldrich, Germany) that has been cut into 5 cm × 5 cm was used for nanofiber deposition. The as-cut ITO-PET piece was placed in the middle of a metal collector dish. Electrical connection between the ITO surface and the underneath metal collector was performed by taping

two aluminum foil stripes at the rims of ITO substrate at the opposite side. This resulted in a final 4 cm x 5 cm collecting area.

After electrospinning conductive electrodes with desired patterns of carbon nanofibers were generated by a CO_2 laser (10.6 µm, Universal Laser Systems, Polytech Systeme GmbH, Germany). The lasing speed was optimized in earlier studies to 60 % (of 1270 mm s^{-1}) and the image density was 1000 DPI. The applied laser power (maximum power of 30 W) was set to 1.5 W if not mentioned otherwise in the respective experimental section.

Morphology characterization

The morphology of nanofibers before and after carbonization was studied by scanning electron microscopy (Zeiss/LEO 1530, Germany) at 5.0 kV. The samples have been cut with a scissor and gold sputtered for 30 s (≈ 7 nm layer thickness) after placing them on specimen stubs. SEM-EDX (Zeiss EVO MA 15 with Bruker XFlash Detector 630M) at 15 kV was applied to demonstrate the elemental composition and distribution along samples. For TEM the LCNF structure of one electrode was scratched off and dispersed in 100 µl water by ultrasonication for 30 s. 2 µl were dropped on a TEM grid placed on a heating plate at 80 °C to enable fast evaporation. Microscopic imaging was performed with a JEOL 2100F with a 4k x 4k camera (UltraScan 4000; Gatan Inc., USA) at 200 kV.

Electrochemical characterization

A CV-50 W Voltammetric Analyzer (Bioanalytical Systems, USA) with a three-electrode system consisting of LCNF as working electrode, Pt wire as counter electrode and a Ag/AgCl reference electrode was utilized for all electrochemical measurements. The working area of LCNF immersed into a measuring solution was defined 2.8 x 3 mm and separated from the

contacting part by the use of candle wax. Cyclic voltammetry was performed from -0.6 V to 1.2 V (50 mV s^{-1}, unless stated otherwise) and amperometry was run at 0.55 V fixed potential. Glucose detection took place in 0.5 M NaOH with gently stirred conditions (ca. 100 rpm).

Mechanical stability test

Electrodeposition on LSG and Fe-LCNFs was performed at -1.0 V for 60 s in aqueous solution of 0.1 M $NaNO_3$ and 0.04 M $Ni(NO_3)_2$. One half of the samples was put into a petri dish, filled with already tempered PBS and incubated at 37 °C for five hours while shaking (50 rpm) to simulate the application in biological media. The other half was kept without incubation as reference for Ni content.

RESULTS AND DISCUSSION

Effect of nickel content on LCNF morphology

Introducing metal salt into spinning solutions leads to changes in the ionic conductivity, typically influencing electrospinnability and fiber morphology.[22] Moreover, nanofibers containing metal salt greatly affect to optimal lasing conditions.[20] Therefore, the influence of Ni content in the spinning solution on the morphology of nanofibers (**Figure 1** a) and laser carbonized nanofibers (**Figure 1** b) was investigated by SEM. Increasing nickel salt from 5 % to 25 % did not show any profound effects on nanofiber mats and fiber diameter (**Figure 1** a). However, the LCNF electrodes after scribing with the same laser settings (1.5 W, 60 % lasing speed) provide differences in morphology (**Figure 1** b). The LCNFs with 25 % Ni showed rather intact homogenous fibrous structures for most of the lasing area while the majority of 5 % and 15 % Ni LCNFs yielded flat/ribbon-like LCNFs with broader diameters compared to that of 25 %

Ni as can be also seen in Figure S1. Here, the diameters of 25 % LCNFs were evaluated and compared with 15 % LCNFs. The expansion of the LCNF diameters compared to the pristine electrospun nanofibers was approximately 20 % and 160 % for 25 % Ni-LCNFs and 15 % Ni-LCNFs, respectively. This might be explained by the fact that increasing metal content promotes greater heat distribution along the nanofibers during the lasing process, thus resulting in the preserved structure similar to the non-scribed nanofibers. We also observed the same heat transfer behavior for LCNFs with varying Fe content in our previous work,[20] in which increase Fe content from 3 % up to 7 % led to greater fibrous structures and became distorted at 10% Fe used. The LCNFs containing 5 % Fe shares similarity in their morphology as obtained from 15 % Ni-LCNF (Figure S2). This suggested that metal salts possess different heat transfer capabilities that need to be taken into consideration in lasing process.

Uniform distribution of nanocatalysts on the electrodes is favorable to enhance electrocatalytic performance. Here, the energy-dispersive X-ray (EDX) mappings have proven that the nickel molecules are distributed evenly over the whole LCNF electrodes at all tested Ni concentrations (**Figure 1** c). It is likely that during electrospinning process Ni salt could be greatly distributed along the electrospun nanofibers, even at 25 % Ni content. Attempts to increase the Ni content higher than 25 % resulted in poor electrospinnability and beaded fibers that subsequently hindered the uniform carbonization of those nanofiber mats (data not shown).

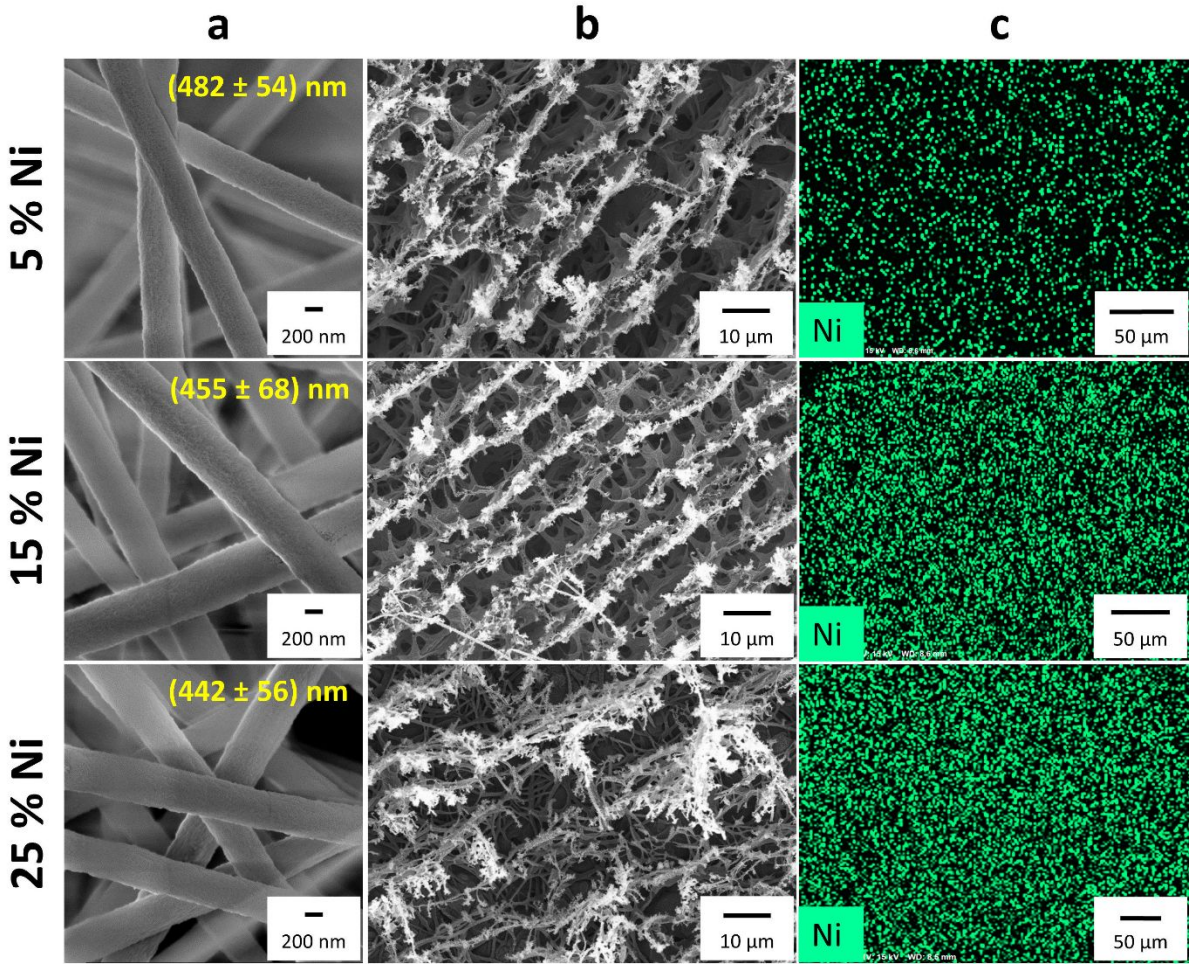

Figure 1. SEM images of electrospun PI nanofibers (a) and LCNF after carbonization for different Ni salt contents (b). EDX elemental mapping showing distribution of nickel molecules for LCNF (c). EDX was recorded with different samples compared to (b).

In order to demonstrate the changes of elemental components of scribed and non-scribed nanofibers, EDX characterization was performed. As illustrated in **Figure 2** i, high density of Ni was observed for both scribed and non-scribed areas (**Figure 2** i-b). This could be anticipated because Ni should not be destroyed by CO_2 laser but transformed into different Ni species. On the other hand, the laser-scribed area displayed higher carbon content (**Figure 2** i-c) and less oxygen content (**Figure 2** i-d) than the non-scribed areas, indicating the successful conversion of

electrospun PI fibers into CNFs. The data are well consistent with the elemental analysis carried out for Fe-LCNF in our previous study.[20]

Apart from EDX mapping, Ni particles embedded within LCNFs and their distribution were characterized by TEM. As can be seen in **Figure 2** ii the particles are distributed evenly along the LCNFs. The Ni particles with mean diameters of (7.9 ± 1.2) nm were achieved by the lasing process which are considerably smaller than the ones obtained from thermal carbonization as shown by Liu *et al.*[10] where approximately 50 nm Ni particles were reported. The smaller Ni particles could lead to greater electrochemical sensitivity due to higher surface area-to-volume ratio. The TEM images shown in **Figure 2** ii a and b and Figure S3 also suggest that favorable distribution of the laser-generated Ni nanoparticles within LCNFs could be achieved from the proposed method. However, it should be noted that under suboptimal spinning conditions, electrospun PI nanofibers containing large agglomerated metal salts can occur. These typically result in LCNFs with defects and poor quality due to non-uniform heat dissipation during laser exposure. The lattice distance of 0.34 nm between the carbon layers shown in **Figure 2** ii-d confirms the formation of graphitic structure in LCNF. The high resolution TEM image (**Figure 2** ii-c) and X-ray diffraction (XRD) spectra (data not shown) suggested that the obtained Ni particles were present in the amorphous form.

Interestingly, further morphological characterizations of 25 % Ni-LCNFs with high magnification SEM suggested that the laser carbonization process transformed the electrospun solid nanofibers containing 25 % Ni (**Figure 2** iii a and b) into hollow-like structure (**Figure 2** iii c and d) where TEM images shown in Figure S3 may also support this hypothesis. Even though the SEM and TEM images indicated hollow-like structures of Ni-LCNFs at first glance, thorough investigation via electron tomography[23] needs to be performed to elucidate whether hollow

structure is obtained in the full length or at least to great extent of LCNFs. This would be of interest for further in-depth study, specially to reveal possible mechanisms and factors that enable hollow-like structure fiber which is typically achieved by sophisticated methods such as core-shell electrospinning.[24] This hollow structure is highly beneficial for developing ultrasensitive sensors, especially for gas sensing, where interactions between analytes and nanocatalysts could take place at the surfaces of outer- and inner walls.[25] High magnification SEM images in **Figure 2** iii c and d and Figure S1 revealed that LCNF walls are non-porous to a large extent. The interconnected pore size of LCNFs estimated from SEM images was (4 ± 3) µm and predominated within the 3D fibrous network. Such pore networks facilitate the accessibility of electroactive species towards the interface.

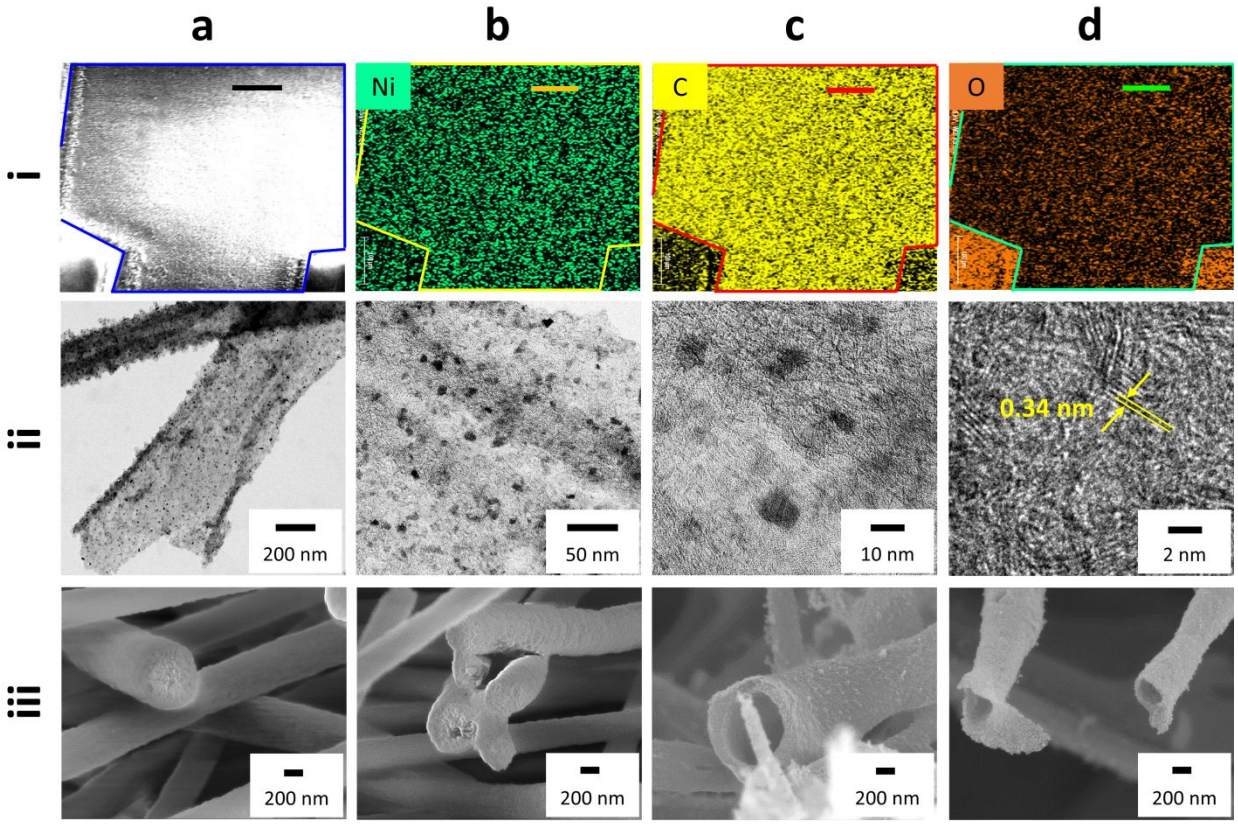

Figure 2. (i) SEM image of LCNF showing the selected field for EDX analysis (a). The lines enclose the carbonized part. Elemental mapping of nickel (b), carbon (c) and oxygen (d) demonstrating the changes in non-scribed and scribed regions. Scale bars are 100 μm. (ii) TEM images of Ni-LCNF at different magnifications. The lattice fringe spacing value of 0.34 nm was determined by TEM software. (iii) SEM images of electrospun solid Matrimid nanofibers (a and b) and hollow LCNFs (c and d). All nanofibers displayed in this figure contain 25 % Ni.

Influence of lasing power on LCNF morphology

The laser power plays a significant role in carbonization process especially with nanofibers embedded with metal salt at various concentrations. **Figure 3** reveals the impact of the laser power on the overall morphology of 25 % Ni-LCNF electrodes after carbonization. The LCNF electrodes scribed at 1.5 W displayed a fully-scribed electrode feature and favorable fibrous structures with high porosity as shown in the top- and side-view of the respective SEM images. The laser power at 0.9 W was insufficient to completely carbonize the whole electrode area while at 1.8 W resulted in electrode burning. As illustrated in the SEM images, the remaining pristine electrospun nanofibers and sheet-like structure were obtained in case of insufficient- and over-carbonized electrodes, respectively. The dependence of lasing power on various Ni concentration was also investigated (Figure S4). As expected, the higher Ni content requires lower lasing power to obtain the desired features of LCNF electrodes, and *vice versa*.

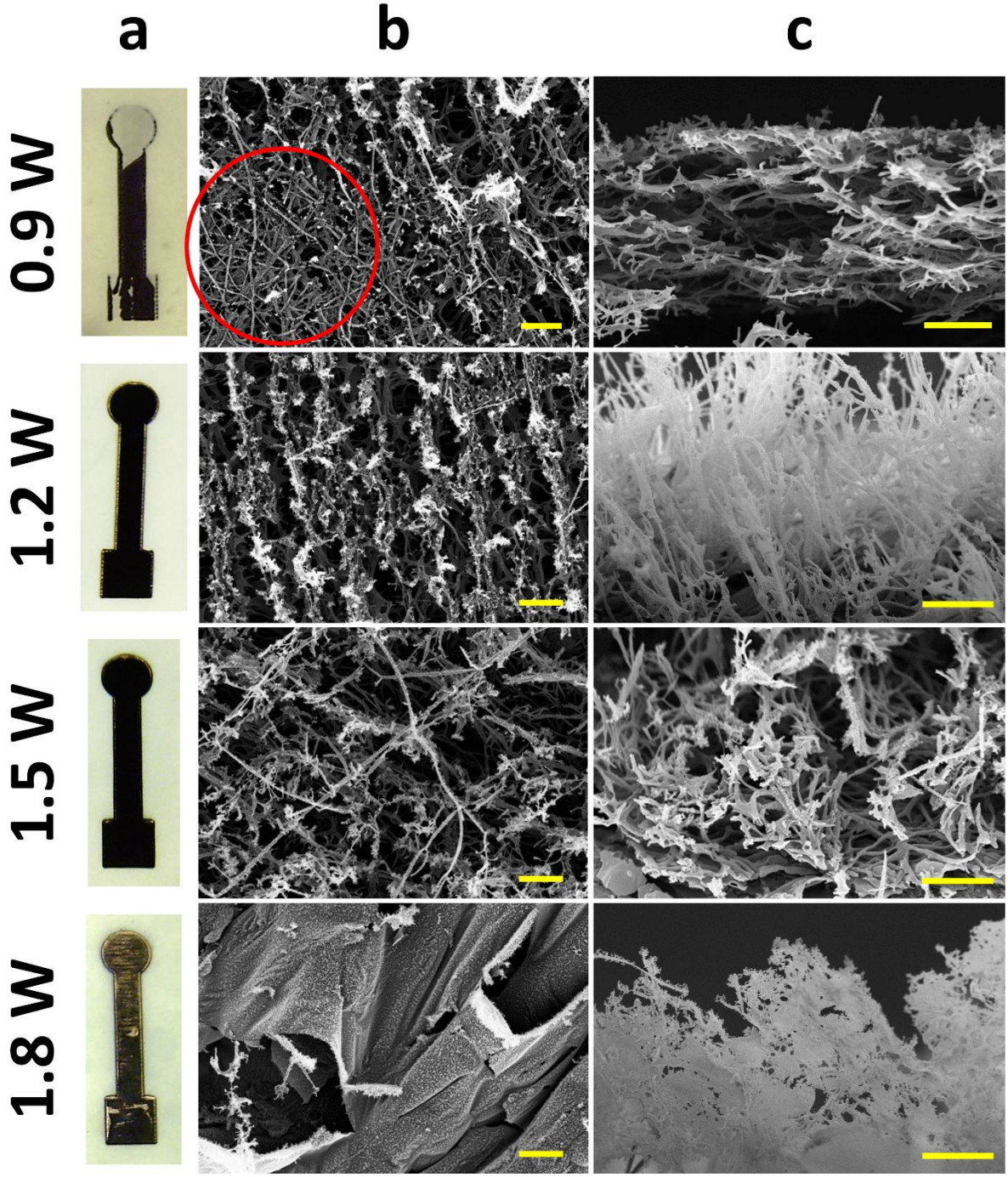

Figure 3. Microscopic images of LCNF electrodes containing 25 % Ni after scribing with 0.9 W, 1.2 W, 1.5 W and 1.8 W laser power (a). Corresponding SEM images for top-view (b) and side-view (c). The scale bars are 10 µm.

Mechanical stability of embedded metal nanocatalysts

In electroanalytical applications, mechanical stability of the embedded nanocatalysts is of great importance as the transducers may encounter stirring conditions or solution flows to promote mass transport. This could subsequently cause the detachment of nanocatalysts from the LCNFs. Therefore, the mechanical stability of the Ni nanoparticles in the LCNFs was assessed by determining the change of Ni content after incubation in PBS solution under shaking at 50 rpm for 5 hr. The EDX data (Figure S5) and **Table 1** reveal a high stability of Ni particles in LCNFs, which is greater than that of the electrodeposited Ni particles on the laser induced graphene (LIG; Kapton foil) and Fe-LCNFs. Here, Ni particles remained stable in LCNF matrix after washing whereas almost 100 % of electrodeposited Ni on LIG and Fe-LCNFs were detached from the electrode surfaces. The strong binding of Ni particles inside LCNFs could be resulted from efficient dispersion of Ni salt during electrospinning and great adhering capability of the Ni complex with PI matrix. In addition, the electrochemical measurement under stirred condition as typically conducted in this work did not lead to any dramatic change in the overall morphology of Ni-LCNFs (Figure S6). Therefore, the strategy is highly suitable to generate CNF-nanocatalyst hybrids for electroanalytical applications, in particular when promoting mass transport through convection is required.

Table 1. Nickel content before and after shaking incubation for different electrodes determined by EDX.

Electrode	Ni content before	Ni content after
LIG w/ eNi	(39.61 ± 1.21) %	(0.83 ± 0.19) %
Fe-LCNF w/ eNi	(40.22 ± 1.19) %	(0.67 ± 0.14) %

Electrode	Ni content before	Ni content after
Ni-LCNF	(6.43 ± 0.76) %	(6.85 ± 0.80) %

Electrochemical glucose sensing

LCNF carrying Ni particles can be exploited in a wide application range. These include electrode material for fuel cells[26] or solar cells[27], supercapacitors for energy storage[28] and organic catalysis[29]. Here, we demonstrate their capability in non-enzymatic sensing of glucose based on electrochemical detection. The electrocatalytic oxidation of glucose by Ni in alkaline medium has been well-established with NaOH being the preferred electrolyte.[30] Figure S7 demonstrates the CV studies of electrocatalytic mechanism by the as-prepared Ni-LCNFs in NaOH. In the absence of glucose (Figure S7 a i and iii), the anodic and cathodic peaks at ca. 500 mV and 300 mV, respectively, are present, indicating the formation of redox couple, $Ni(OH)_2/NiO(OH)$, that typically occurs with Ni-based electrodes in an alkaline medium.[30] This led to the assumption that the laser exposure may induce the formation of NiO rather than the other oxide species, e.g. NiO_2 and Ni_3O_4. The change of one electron process (Ni^{2+}/Ni^{3+}) in the electrocatalytic reaction as described in Figure S7 may also support the formation of NiO, which differs from NiO_2 and Ni_3O_4 where the changes of electron are 2 and 0.67, respectively. Apart from this evidence, the additional peak couples at 660 mV and 620 mV of Ni-LCNFs in ferri/ferro cyanide solution shown in Figure S8 also postulated the formation of NiO during laser exposure as $Ni^{2+}$is generally participated in the generation of nickel hexacyanoferrate (NiHCF) complex ($Ni^{2+} + K_3Fe(CN)_6 \rightarrow KNiFe(CN)_6 + 2K^+ + 2e^-$).[31] Further detailed discussion with respect to the formation of NiHCF can be found in the supporting information (Figure S8). Treating the electrode with 40 CV cycles resulted in the increased peak currents until they

became saturated. This suggests that upon electrochemical treatment the hydrophilicity of Ni-LCNF electrodes increased, enabling the accessibility of analytes inside the porous structure. The presence of glucose results in the increased oxidative peak and anodic shift towards 550 mV, attributing to the electrocatalytic oxidation of glucose to gluconolactone by NiO(OH) (Figure S7 a ii). The generated anodic peaks were proportional to the concentrations of glucose (Figure S7 b). The linearity between the peak currents and square root of scan rates revealed the diffusion-based reaction of NaOH and glucose occurred at the Ni-LCNFs. These results are consistent with those reported in the literature,[32–34] suggesting that the expected electrocatalytic behavior can be realized from the laser-generated Ni hybrid. The sensing mechanism is detailed in the supporting information (Figure S7).

The effects of Ni content in electrospun PI nanofibers on electrochemical performance of glucose sensing were investigated by amperometry at 550 mV. As expected, the higher amount of Ni content facilitates a greater sensitivity for glucose sensing (**Figure 4** a). It is assumed that 25 % Ni content promotes a larger number of laser-generated nanocatalysts exposed to the LCNF surface than that of 15 % and 5 %. It is also possible that the remarkable current response obtained from 25% Ni-LCNFs might be also attributed to the enhanced electroactive surface area (ESA) offered by the intact fibrous feature (**Figure 1** b 25 % Ni). As can be seen in Figure S8, the 25 % Ni-LCNF electrodes possess an ESA of approx. 1.3-times and 3.1-times higher that of 15 % Ni-LCNFs and 5 % Ni-LCNFs, respectively. The result implies that high Ni content loaded in LCNFs plays a more important role in the enhanced sensitivity than the increased ESA as the sensitivity of glucose sensing offered by 25 % Ni-LCNF electrodes is ca. 4.7-times and 9.9-times higher than that of 15 % Ni-LCNF and 5 % Ni-LCNF, respectively. However, we believe that the fibrous-like morphology obtained from 25 % Ni-LCNF not only contributes to higher

collision rates between Ni nanoparticles and glucose but also facilitates the fast response time as can been seen from rapid signal rising within 5 s after glucose injection. In summary, the combination of high content of nanocatalysts together with the obtained fibrous-like structures leads to a large surface area with exposed functional nanocatalysts, which is thought to be the main reason for the significant boost in electrochemical performance of 25 % Ni-LCNF compared to 5 % and 15 %. In addition, the inset of **Figure 4** a clearly indicates that the electrocatalytic oxidation of glucose is specifically resulted from Ni nanoparticles as LCNFs carrying 5 % Fe did not provide any significant signal response upon glucose injection. Furthermore, we found that various lasing power not only generates 25 % Ni-LCNFs with distinct morphological structures but also greatly affects to the sensitivity of glucose sensing as shown in Figure S9. Here, lasing the nanofibers with 1.5 W enabled the maximum signal current of glucose sensing which could also be attributed to the obtained intact fibrous LCNFs (**Figure 3**).

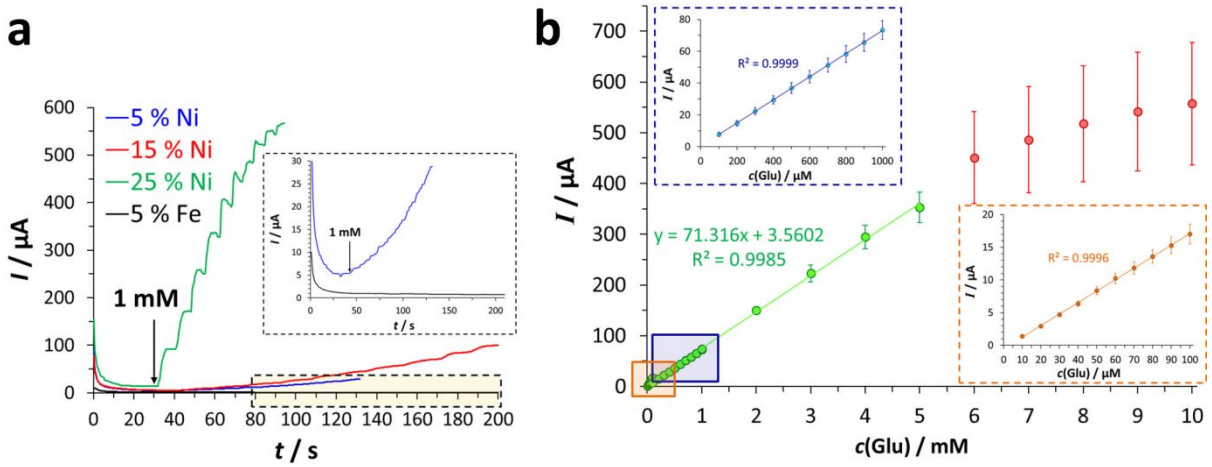

Figure 4. Amperometric response of LCNF containing different concentrations of Ni (5 %, 15 %, 25 %) and 5 % Fe as control towards glucose injection (a). One injection step equals 1 mM glucose. Dose-response upon glucose injection in 10 µM steps (0-100 µM), 100 µM steps (100-

1,000 μM) and 1,000 μM steps (1,000-10,000 μM) (n≥3) (b). The potential was fixed at 0.55 V and the detection matrix consisted of 0.5 M NaOH.

The sensitivity of 25 % Ni-LCNF electrodes was further investigated as shown in **Figure 4** b. The sensitivity towards glucose reaches up to 2092 μA mM^{-1} cm^{-2} and 857 μA mM^{-1} cm^{-2} for the linear range of 10-100 μM and 100 μM to 5 mM, respectively. The limit of detection (LOD) as low as 0.3 μM could be achieved. The obtained large dynamic range covers the range of glucose in several human body fluids (ocular fluid, urine, saliva and sweat).[35,36] Electrode poisoning by halides, e.g. Cl^-, is a major problem in glucose detection based non-enzymatic electrochemical sensors.[30,37,38] However, as shown in Figure S10, the presence of Cl^- in detection medium even up to 250 mM did not notably interfere with the sensing performance. A comparison of our material towards glucose sensing with other existing composites that are also based on nickel-carbon composites is given in **Table 2**. Our LCNF-Ni electrode not only provides excellent analytical performance highly competitive to the other reports but also possesses superior characteristics, especially, in terms of its simplicity, flexibility, affordability, and mass-production capability.

Table 2. Comparison of the analytical performance of most recent nickel-carbon hybrid materials towards non-enzymatic glucose sensing.

Material	Linear range / μM	LOD / μM	Sensitivity / μA mM^{-1} cm^{-2}	Reference
Nano NiO processed by potential scan	1-10	0.16	66.0	[39]
	1-110		55.9	
NiNP/SMWNTs	1-1,000	0.5	1,438	[40]
$Ni(OH)_2$-graphene	1-10	0.6	494	[41]

Material	Linear range / μM	LOD / μM	Sensitivity / μA mM^{-1} cm^{-2}	Reference
	10-1,000		328	
NiO/OMC/GCE	2-1,000	0.65	834.8	[42]
CNT-Ni nanocomposite	5-2,000	2	1,384.1	[43]
NiONP/PANiNW/GO/GCE	2-960	0.5	376.22	[44]
	960-5,560			
NiNPs/ATP/RGO	1-710	0.37	1,414.4	[45]
3-D/Ni-Fe nanosheets	0.05-200	0.031	7.90	[46]
NiO-HAC	10-3,300	1	199.86	[47]
$Ni(OH)_2$/CNT fiber microelectrodes	20-10,500	0.645	12,200	[48]
PF/Ni30	20-500	8	670	[49]
Ni-Pd@AC/GCE	10-1,000	0.014	90,000	[50]
Ni/NC-800	2-4,658	0.12	660.3	[51]
Ni-LCNF	10-100	0.3	2,092	this work
	100-5,000		857	

Apart from sensitivity, various Ni content in LCNFs also affects the selectivity of glucose sensing. As can be seen from **Figure 5** a and c, 25 % Ni is high enough to selectively enable the electrocatalytic response of glucose for both 1 mM and 100 μM without interfering effects from uric acid (UA) and ascorbic acid (AA). On the other hand, the current responses of interferent species obtained from 5 % and 15 % Ni are non-negligible when compared to the glucose (**Figure 5** b and **Figure 5** d). It is possible that the oxidations of UA and AA were prone to take place at carbon surface generating high signal response, especially at 5 % Ni (**Figure 5** d). It should be noted that higher concentrations of UA and AA may possibly interfere the sensing performance of Ni-LCNFs, which is considered as an inherent problem for general non-

enzymatic electrochemical sensors. However, other studies demonstrated a viable solution to this problem, e.g. using semipermeable membrane as a protective layer.[52,53]

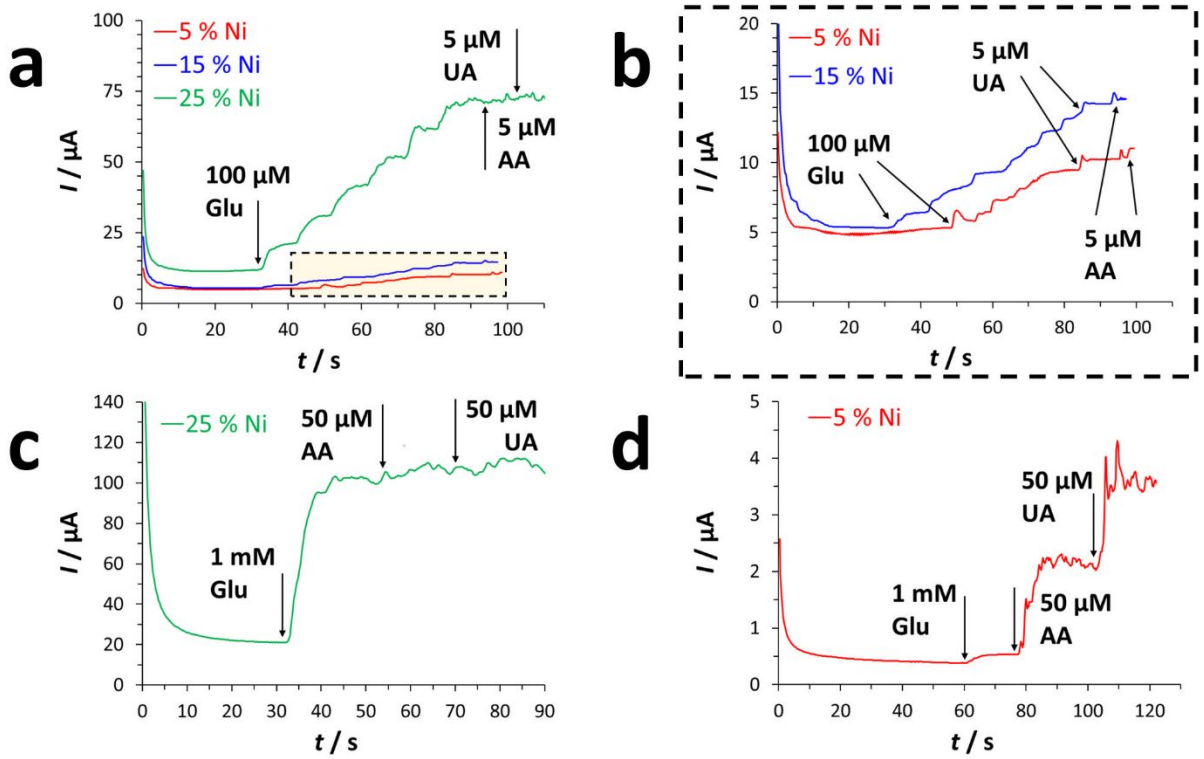

Figure 5. Amperometric response of LCNF containing different percentages of Ni towards successive 100 µM glucose (Glu) addition and final addition of potential interferents ascorbic acid (AA) and uric acid (UA) (both 5 µM) (n=3) (a). Zoom-in of the amperograms for 5/15 % Ni content with noticeable steps after addition of interferents (b). Amperometric response of LCNF containing 25 % Ni (c) and 5 % Ni (d) after addition of 1 mM Glu and 50 µM of AA and UA each. For 5 % Ni the signal of both interferents are significantly higher than that of glucose, whereas for 25 % Ni only glucose leads to a signal. The potential was fixed at 0.55 V and the detection matrix consisted of 0.5 M NaOH. In case of fluctuating signals the mean value was taken for evaluation.

CONCLUSIONS

Generating carbon nanofibers with embedded metal nanocatalysts can be easily achieved by a one-step laser-induced carbonization of electrospun nanofibers containing metal complex. Our strategy provides 3D architecture of carbon nanofiber networks with embedded ultrasmall and uniform distribution of metal nanoparticles. The nanoparticles adhere firmly within carbon nanofibers. Undoubtedly, the as-prepared hybrids exhibit excellent performance towards non-enzymatic glucose sensing, especially in terms of sensitivity and selectivity. By changing the metal complex, carbon nanofiber with a variety of metal nanocatalysts can be created. Apart from favorable electrocatalytic performance, extremely low material cost ($ 0.07 per electrode), fast manufacturing process, and high flexibility in terms of electrode designs and type of incorporated metal nanocatalysts are additional characteristics that make this strategy ideal for large-scale production and commercialization. This opens up an opportunity to efficiently miniaturize and integrate electrochemical devices with nanocatalysts useful for many relevant applications, especially in domains of (bio)sensing, energy-storage, synthetic chemistry or (bio)medicine.

ASSOCIATED CONTENT

Supporting Information

The Supporting Information is available free of charge.

Morphology of Ni-LCNFs with varying nickel content; morphology of Ni-LCNFs *vs.* Fe-LCNFs; TEM images of 25 % Ni-LCNFs; lasing power and Ni content variation; EDX spectra for mechanical stability experiment; mechanical stability of Ni-LCNFs after electrochemical measurement under stirred condition; cyclic voltammetry glucose mechanism study;

electrochemical surface area at varying Ni content; glucose response for Ni-LCNF prepared with varying lasing power; glucose response for Ni-LCNF in NaOH w/ and w/o NaCl

AUTHOR INFORMATION

Corresponding Author

*Nongnoot Wongkaew. E-Mail: nongnoot.wongkaew@ur.de

Author Contributions

M. Simsek and N. Wongkaew conceived the studies and wrote the manuscript. A. J. Baeumner led the project administration and promoted manuscript preparation. M. Simsek performed the experiments. M. Schlosser carried out EDX measurements. K. Hoecherl supported experiment implementation and validation. All authors have given approval to the final version of the manuscript.

Funding Sources

The work was supported in part by the King Abdullah University of Science and Technology (KAUST).

Notes

There are no conflicts of interest to declare.

ACKNOWLEDGMENT

The authors would like to thank Prof. Dr. Reinhard Rachel for the help on the TEM imaging.

ABBREVIATIONS

3D, three dimensional; AA, ascorbic acid; CNF, carbon nanofiber; EDX, energy-dispersive X-ray; Glu, glucose; $Ni(acac)_2$, LCNF, laser induced carbon nanofiber; LOD, limit of detection; nickel acetylacetonate; PI, polyimide: SEM, scanning electron microscopy; TEM, transmission electron microscopy; UA, uric acid; XRD, X-ray diffraction.

REFERENCES

(1) Browne, M. P.; Redondo, E.; Pumera, M. 3D Printing for Electrochemical Energy Applications. *Chem. Rev.* **2020**, *120* (5), 2783–2810.

(2) Wang, Z.; Wu, S.; Wang, J.; Yu, A.; Wei, G. Carbon Nanofiber-Based Functional Nanomaterials for Sensor Applications. *Nanomaterials* **2019**, *9* (7), 1045.

(3) Chinthaginjala, J. K.; Seshan, K.; Lefferts, L. Preparation and Application of Carbon-Nanofiber Based Microstructured Materials as Catalyst Supports. *Ind. Eng. Chem. Res.* **2007**, *46* (12), 3968–3978.

(4) Nantaphol, S.; Watanabe, T.; Nomura, N.; Siangproh, W.; Chailapakul, O.; Einaga, Y. Bimetallic Pt–Au Nanocatalysts Electrochemically Deposited on Boron-Doped Diamond Electrodes for Nonenzymatic Glucose Detection. *Biosens. Bioelectron.* **2017**, *98*, 76–82.

(5) Wang, Y.; He, Q.; Guo, J.; Wei, H.; Ding, K.; Lin, H.; Bhana, S.; Huang, X.; Luo, Z.; Shen, T. D.; et al. Carboxyl Multiwalled Carbon-Nanotube-Stabilized Palladium Nanocatalysts toward Improved Methanol Oxidation Reaction. *ChemElectroChem* **2015**, *2*, 559–570.

(6) Khalily, M. A.; Yurderi, M.; Haider, A.; Bulut, A.; Patil, B.; Zahmakiran, M.; Uyar, T. Atomic Layer Deposition of Ruthenium Nanoparticles on Electrospun Carbon Nanofibers: A Highly Efficient Nanocatalyst for the Hydrolytic Dehydrogenation of Methylamine Borane. *ACS Appl. Mater. Interfaces* **2018**, *10*, 26162–26169.

(7) Sahin, O. G. Microwave-Assisted Synthesis of PtAu@C Based Bimetallic Nanocatalysts for Non-Enzymatic H_2O_2 Sensor. *Electrochim. Acta* **2015**, *180*, 873–879.

(8) Inagaki, M.; Yang, Y.; Kang, F. Carbon Nanofibers Prepared via Electrospinning. *Advanced Materials*. 2012, pp 2547–2566.

(9) Liu, D.; Guo, Q.; Hou, H.; Niwa, O.; You, T. PdxCoy Nanoparticle/Carbon Nanofiber Composites with Enhanced Electrocatalytic Properties. *ACS Catal.* **2014**, *4* (6), 1825–1829.

(10) Liu, Y.; Teng, H.; Hou, H.; You, T. Nonenzymatic Glucose Sensor Based on Renewable Electrospun Ni Nanoparticle-Loaded Carbon Nanofiber Paste Electrode. *Biosens. Bioelectron.* **2009**, *24* (11), 3329–3334.

(11) Yang, T.; Zhu, H.; Wan, M.; Dong, L.; Zhang, M.; Du, M. Highly Efficient and Durable PtCo Alloy Nanoparticles Encapsulated in Carbon Nanofibers for Electrochemical Hydrogen Generation. *Chem. Commun.* **2016**, *52* (5), 990–993.

(12) Huang, J.; Wang, D.; Hou, H.; You, T. Electrospun Palladium Nanoparticle-Loaded Carbon Nanofibers and Their Electrocatalytic Activities towards Hydrogen Peroxide and NADH. *Adv. Funct. Mater.* **2008**, *18* (3), 441–448.

(13) Lee, J. S.; Kwon, O. S.; Park, S. J.; Park, E. Y.; You, S. A.; Yoon, H.; Jang, J. Fabrication of Ultrafine Metal-Oxide-Decorated Carbon Nanofibers for DMMP Sensor Application. *ACS Nano* **2011**, *5* (10), 7992–8001.

(14) Guo, Q.; Liu, D.; Zhang, X.; Li, L.; Hou, H.; Niwa, O.; You, T. Pd–Ni Alloy Nanoparticle/Carbon Nanofiber Composites: Preparation, Structure, and Superior Electrocatalytic Properties for Sugar Analysis. *Anal. Chem.* **2014**, *86* (12), 5898–5905.

(15) Guan, H.; Zhao, Y.; Zhang, J.; Liu, Y.; Yuan, S.; Zhang, B. Uniformly Dispersed PtNi Alloy Nanoparticles in Porous N-Doped Carbon Nanofibers with High Selectivity and Stability for Hydrogen Peroxide Detection. *Sensors Actuators B Chem.* **2018**, *261*, 354–363.

(16) Zhang, P.; Wang, F.; Yu, M.; Zhuang, X.; Feng, X. Two-Dimensional Materials for Miniaturized Energy Storage Devices: From Individual Devices to Smart Integrated Systems. *Chem. Soc. Rev.* **2018**, *47* (19), 7426–7451.

(17) Lv, Z.; Li, W.; Yang, L.; Loh, X. J.; Chen, X. Custom-Made Electrochemical Energy Storage Devices. *ACS Energy Lett.* **2019**, *4* (2), 606–614.

(18) Zarei, M. Portable Biosensing Devices for Point-of-Care Diagnostics: Recent Developments and Applications. *TrAC Trends Anal. Chem.* **2017**, *91*, 26–41.

(19) Kim, J.; Campbell, A. S.; de Ávila, B. E.-F.; Wang, J. Wearable Biosensors for Healthcare Monitoring. *Nat. Biotechnol.* **2019**, *37* (4), 389–406.

(20) Wongkaew, N.; Simsek, M.; Arumugam, P.; Behrent, A.; Berchmans, S.; Baeumner, A. J. A Robust Strategy Enabling Addressable Porous 3D Carbon-Based Functional Nanomaterials in Miniaturized Systems. *Nanoscale* **2019**, *11*, 3674–3680.

(21) Ye, R.; Peng, Z.; Wang, T.; Xu, Y.; Zhang, J.; Li, Y.; Nilewski, L. G.; Lin, J.; Tour, J. M. In Situ Formation of Metal Oxide Nanocrystals Embedded in Laser-Induced Graphene. *ACS Nano* **2015**, *9* (9), 9244–9251.

(22) Yalcinkaya, F.; Yalcinkaya, B.; Jirsak, O. Influence of Salts on Electrospinning of Aqueous and Nonaqueous Polymer Solutions. *J. Nanomater.* **2015**, *2015*, 134251.

(23) Frank, J. *Electron Tomography: Methods for Three-Dimensional Visualization of Structures in the Cell*; Springer New York, 2008.

(24) Ding, B.; Wang, M.; Wang, X.; Yu, J.; Sun, G. Electrospun Nanomaterials for Ultrasensitive Sensors. *Mater. Today* **2010**, *13* (11), 16–27.

(25) Choi, S.-H.; Ankonina, G.; Youn, D.-Y.; Oh, S.-G.; Hong, J.-M.; Rothschild, A.; Kim, I.-D. Hollow ZnO Nanofibers Fabricated Using Electrospun Polymer Templates and Their Electronic Transport Properties. *ACS Nano* **2009**, *3* (9), 2623–2631.

(26) Khare, P.; Ramkumar, J.; Verma, N. Carbon Nanofiber-Skinned Three Dimensional Ni/Carbon Micropillars: High Performance Electrodes of a Microbial Fuel Cell. *Electrochim. Acta* **2016**, *219*, 88–98.

(27) Zhou, Z.; Sigdel, S.; Gong, J.; Vaagensmith, B.; Elbohy, H.; Yang, H.; Krishnan, S.; Wu, X.-F.; Qiao, Q. Graphene-Beaded Carbon Nanofibers with Incorporated Ni Nanoparticles as Efficient Counter-Electrode for Dye-Sensitized Solar Cells. *Nano Energy* **2016**, *22*, 558–563.

(28) Zhang, C.; Chen, Q.; Zhan, H. Supercapacitors Based on Reduced Graphene Oxide Nanofibers Supported $Ni(OH)_2$ Nanoplates with Enhanced Electrochemical Performance. *ACS Appl. Mater. Interfaces* **2016**, *8* (35), 22977–22987.

(29) van Haasterecht, T.; Ludding, C. C. I.; de Jong, K. P.; Bitter, J. H. Toward Stable Nickel Catalysts for Aqueous Phase Reforming of Biomass-Derived Feedstock under Reducing and Alkaline Conditions. *J. Catal.* **2014**, *319*, 27–35.

(30) Wang, G.; He, X.; Wang, L.; Gu, A.; Huang, Y.; Fang, B.; Geng, B.; Zhang, X. Non-Enzymatic Electrochemical Sensing of Glucose. *Microchimica Acta*. 2013, pp 161–186.

(31) Tawfic, A.; Dickson-Anderson, S.; Kim, Y.; Mekky, W.; Baraka, A.; Gobara, M. Preparation and Characterization of Nickel Hexacyanoferrate Films for the Removal of Cesium Ion by Electrically Switched Ion Exchange (ESIX). *J. Solid State Electrochem.* **2017**.

(32) Zhan, B.; Liu, C.; Chen, H.; Shi, H.; Wang, L.; Chen, P.; Huang, W.; Dong, X. Free-Standing Electrochemical Electrode Based on $Ni(OH)_2$/3D Graphene Foam for Nonenzymatic Glucose Detection. *Nanoscale* **2014**, *6* (13), 7424–7429.

(33) Zhang, X.; Xu, Y.; Ye, B. An Efficient Electrochemical Glucose Sensor Based on Porous Nickel-Based Metal Organic Framework/Carbon Nanotubes Composite (Ni-MOF/CNTs).

J. Alloys Compd. **2018**, *767*, 651–656.

(34) Rezaeinasab, M.; Benvidi, A.; Tezerjani, M. D.; Jahanbani, S.; Kianfar, A. H.; Sedighipoor, M. An Electrochemical Sensor Based on Ni(II) Complex and Multi Wall Carbon Nano Tubes Platform for Determination of Glucose in Real Samples. *Electroanalysis* **2017**, *29* (2), 423–432.

(35) Bruen, D.; Delaney, C.; Florea, L.; Diamond, D. Glucose Sensing for Diabetes Monitoring: Recent Developments. *Sensors* **2017**, *17*, 1–21.

(36) Nery, E. W.; Kundys, M.; Jeleń, P. S.; Jönsson-Niedziólka, M. Electrochemical Glucose Sensing: Is There Still Room for Improvement? *Anal. Chem.* **2016**, *88*, 11271–11282.

(37) Argyle, M. D.; Bartholomew, C. H. Heterogeneous Catalyst Deactivation and Regeneration: A Review. *Catalysts* **2015**, *5*, 145–269.

(38) El-Refaei, S. M.; Saleh, M. M.; Awad, M. I. Tolerance of Glucose Electrocatalytic Oxidation on NiOx/MnOx/GC Electrode to Poisoning by Halides. *J. Solid State Electrochem.* **2014**, *18* (1), 5–12.

(39) Mu, Y.; Jia, D.; He, Y.; Miao, Y.; Wu, H. L. Nano Nickel Oxide Modified Non-Enzymatic Glucose Sensors with Enhanced Sensitivity through an Electrochemical Process Strategy at High Potential. *Biosens. Bioelectron.* **2011**, *26*, 2948–2952.

(40) Nie, H.; Yao, Z.; Zhou, X.; Yang, Z.; Huang, S. Nonenzymatic Electrochemical Detection of Glucose Using Well-Distributed Nickel Nanoparticles on Straight Multi-Walled Carbon Nanotubes. *Biosens. Bioelectron.* **2011**, *30*, 28–34.

(41) Qiao, N.; Zheng, J. Nonenzymatic Glucose Sensor Based on Glassy Carbon Electrode Modified with a Nanocomposite Composed of Nickel Hydroxide and Graphene. *Microchim. Acta* **2012**, *177*, 103–109.

(42) Luo, L.; Li, F.; Zhu, L.; Ding, Y.; Zhang, Z.; Deng, D.; Lu, B. Nonenzymatic Glucose Sensor Based on Nickel(II)Oxide/Ordered Mesoporous Carbon Modified Glassy Carbon Electrode. *Colloids Surfaces B Biointerfaces* **2013**, *102*, 307–311.

(43) Choi, T.; Kim, S. H.; Lee, C. W.; Kim, H.; Choi, S. K.; Kim, S. H.; Kim, E.; Park, J.; Kim, H. Synthesis of Carbon Nanotube-Nickel Nanocomposites Using Atomic Layer Deposition for High-Performance Non-Enzymatic Glucose Sensing. *Biosens. Bioelectron.* **2015**, *63*, 325–330.

(44) Zhuang, X.; Tian, C.; Luan, F.; Wu, X.; Chen, L. One-Step Electrochemical Fabrication of a Nickel Oxide Nanoparticle/Polyaniline Nanowire/Graphene Oxide Hybrid on a Glassy Carbon Electrode for Use as a Non-Enzymatic Glucose Biosensor. *RSC Adv.* **2016**, *6*, 92541–92546.

(45) Shen, Z.; Gao, W.; Li, P.; Wang, X.; Zheng, Q.; Wu, H.; Ma, Y.; Guan, W.; Wu, S.; Yu, Y.; et al. Highly Sensitive Nonenzymatic Glucose Sensor Based on Nickel Nanoparticle-Attapulgite-Reduced Graphene Oxide-Modified Glassy Carbon Electrode. *Talanta* **2016**, *159*, 194–199.

(46) Kannan, P.; Maiyalagan, T.; Marsili, E.; Ghosh, S.; Niedziolka-Jönsson, J.; Jönsson-Niedziolka, M. Hierarchical 3-Dimensional Nickel-Iron Nanosheet Arrays on Carbon Fiber Paper as a Novel Electrode for Non-Enzymatic Glucose Sensing. *Nanoscale* **2016**,

8, 843–855.

(47) Ni, Y.; Xu, J.; Liang, Q.; Shao, S. Enzyme-Free Glucose Sensor Based on Heteroatom-Enriched Activated Carbon (HAC) Decorated with Hedgehog-like NiO Nanostructures. *Sensors Actuators, B Chem.* **2017**, *250*, 491–498.

(48) Qian, Q.; Hu, Q.; Li, L.; Shi, P.; Zhou, J.; Kong, J.; Zhang, X.; Sun, G.; Huang, W. Sensitive Fiber Microelectrode Made of Nickel Hydroxide Nanosheets Embedded in Highly-Aligned Carbon Nanotube Scaffold for Nonenzymatic Glucose Determination. *Sensors Actuators, B Chem.* **2018**, *257*, 23–28.

(49) Marini, S.; Ben Mansour, N.; Hjiri, M.; Dhahri, R.; El Mir, L.; Espro, C.; Bonavita, A.; Galvagno, S.; Neri, G.; Leonardi, S. G. Non-Enzymatic Glucose Sensor Based on Nickel/Carbon Composite. *Electroanalysis* **2018**, *30* (4), 727–733.

(50) Koskun, Y.; Şavk, A.; Şen, B.; Şen, F. Highly Sensitive Glucose Sensor Based on Monodisperse Palladium Nickel/Activated Carbon Nanocomposites. *Anal. Chim. Acta* **2018**, *1010*, 37–43.

(51) Gao, W.; Li, Q.; Dou, M.; Zhang, Z.; Wang, F. Self-Supported Ni Nanoparticles Embedded on Nitrogen-Doped Carbon Derived from Nickel Polyphthalocyanine for High-Performance Non-Enzymatic Glucose Detection. *J. Mater. Chem. B* **2018**, *6*, 6781–6787.

(52) Kulkarni, T.; Slaughter, G. Application of Semipermeable Membranes in Glucose Biosensing. *Membranes* . 2016.

(53) Park, S.; Jeong, R.-A.; Boo, H.; Park, J.; Kim, H. C.; Chung, T. D. Nonenzymatic

Continuous Glucose Monitoring in Human Whole Blood Using Electrified Nanoporous Pt. *Biosens. Bioelectron.* **2012**, *31*, 284–291.

Table of Contents